

Article

High-Performance Computational Method for an Extended Three-Coupled Korteweg–de Vries System

Panpan Wang and Xiufang Feng *

School of Mathematics and Statistics, Ningxia University, Yinchuan 750021, China; 12022140038@stu.nxu.edu.cn
* Correspondence: xf_feng@nxu.edu.cn

Abstract: This paper calculates numerical solutions of an extended three-coupled Korteweg–de Vries system by the q-homotopy analysis transformation method (q-HATM), which is a hybrid of the Laplace transform and the q-homotopy analysis method. Multiple investigations inspecting planetary oceans, optical cables, and cosmic plasma have employed the KdV model, significantly contributing to its development. The uniqueness, convergence, and maximum absolute truncation error of this algorithm are demonstrated. A numerical simulation has been performed to validate the accuracy and validity of the proposed approach. With high accuracy and few algorithmic processes, this algorithm supplies a series solution in the form of a recursive relation.

Keywords: an extended three-coupled Korteweg–de Vries system; the Laplace transform; numerical solutions; numerical simulation; the q-homotopy analysis transformation method

MSC: 35A08, 35C07



Citation: Wang, P.; Feng, X. High-Performance Computational Method for an Extended Three-Coupled Korteweg–de Vries System. *Axioms* **2023**, *12*, 990. <https://doi.org/10.3390/axioms12100990>

Academic Editors: Pengzhan Huang, Yinnian He and Patricia J. Y. Wong

Received: 31 August 2023
Revised: 10 October 2023
Accepted: 12 October 2023
Published: 19 October 2023



Copyright: © 2023 by the authors. Licensee MDPI, Basel, Switzerland. This article is an open access article distributed under the terms and conditions of the Creative Commons Attribution (CC BY) license (<https://creativecommons.org/licenses/by/4.0/>).

1. Introduction

In the past two decades, nonlinear science has begun to appear in modern mathematics, physics, engineering technology, and other important fields [1–4]. Presently, the primary topic of research in many categories, which include natural science and engineering technology, has shifted from linear problems to nonlinear problems. Such a form of complex problem necessitates extensive research and faces distinct difficulties. However, the study of nonlinear PDEs [5–9] has already started to encounter problems. In physics, fluid mechanics, communication technology, material science, dynamical systems, and biology, nonlinear coupled PDEs are commonly implemented. As a consequence, understanding how to solve nonlinear PDEs has both important theoretical and practical consequences.

Traditional numerical methods require more computer memory to calculate numerical solutions. This means that the semi-analytical technique and the Laplace transform eliminate the time-consuming drawbacks and need less CPU processing time while analyzing the numerical solutions of nonlinear phenomena in the actual world. A hybrid of the homotopy polynomials, the Laplace transform, and the q-HAM [10–14] is the q-HATM [15–19]. We analyze the uniqueness, convergence, and utmost absolute error [20,21] of q-HATM solutions. This algorithm has the advantages of both methods.

This article is going to investigate the extended three-coupled Korteweg–de Vries system [22–24],

$$\begin{aligned}u_t &= \beta_1 u_{xxx} + \beta_2 u_x v + \beta_2 u v_x, \\v_t &= \beta_1 \beta_3 v_{xxx} + 2\beta_2 \beta_3 v v_x - \beta_2 w_x, \\w_t &= \beta_1 w_{xxx} + \beta_2 v w_x - 2\beta_2 u u_x,\end{aligned}\tag{1}$$

with real differentiable functions associated with variables x and t including u , v , and w , while β_1 , β_2 , and β_3 are three non-zero real constants. In investigations of planetary oceans, optical fibers, and cosmic plasma, the KdV model has been extensively employed.

The main framework of this paper is as follows. The fundamental concepts of the sub-equation method [25–27] and the q-HATM are outlined in Section 2; the uniqueness and convergence of numerical solutions are also confirmed. The extended three-coupled Korteweg–de Vries system is discussed in Section 3 along with its analytical and numerical solutions. Section 4 shows the numerical results and comments. Section 5 concludes by providing some recommendations and outlining the key findings.

2. Analysis of the Presented Methodology

2.1. The Sub Equation Method

The Riccati equation is the foundation of the sub equation approach,

$$\psi'(\eta) = \alpha + \psi^2(\eta). \tag{2}$$

When it comes to a particular PDE with two variables,

$$F(x, t, u_t, u_x, u_{xx}, \dots) = 0, \tag{3}$$

the travelling wave solution [25–27] is

$$\eta = bt + x, \quad u(x, t) = U(\eta), \tag{4}$$

in this case, b is a constant that will be explained further.

Substituting Equation (4) into Equation (3), the following equation is established,

$$G(U(\eta), U'(\eta), \dots) = 0. \tag{5}$$

Presumptive analytical solutions of Equation (5) are as follows:

$$U(\eta) = \sum_{i=0}^N a_i \psi^i(\eta), \quad a_N \neq 0, \tag{6}$$

The principle of balance can be employed for estimating a positive integer N , and the coefficients a_i ($0 \leq i \leq N$) will be calculated afterward.

Equation (2) possesses five types of analytical solutions, which are listed below,

$$\psi(\eta) = \begin{cases} -\sqrt{-\alpha} \tanh(\sqrt{-\alpha}\eta), & \alpha < 0, \\ -\sqrt{-\alpha} \coth(\sqrt{-\alpha}\eta), & \alpha < 0, \\ -\frac{1}{\eta}, & \alpha = 0, \\ \sqrt{\alpha} \tan(\sqrt{\alpha}\eta), & \alpha > 0, \\ -\sqrt{\alpha} \cot(\sqrt{\alpha}\eta), & \alpha > 0. \end{cases} \tag{7}$$

With the help of the previously mentioned results, we can formulate equations for b and a_i ($i = 1, 2, \dots, N$) by juggling the coefficients of a polynomial describing $\psi(\eta)$. Then, we get the analytical solutions of Equation (3).

2.2. Fundamental Plan of the q-HATM

The following introduces [15–19] the basic idea of the q-HATM for nonlinear PDEs, assuming that the PDEs have the following form,

$$u_t(x, t) + Nu(x, t) + Ru(x, t) = f(x, t), \tag{8}$$

where N is Lipschitz continuous and a nonlinear differential operator. The linear differential operator R is bounded, meaning that given a number μ , we acquire $\|Ru\| \leq \mu \|u\|$. The source term is $f(x, t)$. Applying the Laplace transform to Equation (8), we have

$$s\mathcal{L}[u(x, t)] + \mathcal{L}[Nu(x, t)] + \mathcal{L}[Ru(x, t)] = u(x, 0) + \mathcal{L}[f(x, t)], \tag{9}$$

The simplification of Equation (9) gives

$$\mathcal{L}[u(x, t)] + \frac{1}{s}\mathcal{L}[Nu(x, t) + Ru(x, t) - f(x, t)] - \frac{1}{s}u(x, 0) = 0. \tag{10}$$

The following is the nonlinear operator,

$$\mathcal{B}[\Theta(x, t; q)] = \mathcal{L}[\Theta(x, t; q)] + \frac{1}{s}\mathcal{L}[N\Theta(x, t; q) + R\Theta(x, t; q) - f(x, t)] - \frac{1}{s}\Theta(x, t; q)(0^+), \tag{11}$$

where the real function of q , x , and t is $\Theta(x, t; q)$ and $q \in [0, \frac{1}{n}]$ ($n \geq 1$) is an embedding parameter. The q-HATM supplies the following non-zero auxiliary function,

$$(1 - nq)\mathcal{L}[\Theta(x, t; q) - u_0(x, t)] = \hbar q H(x, t)\mathcal{B}[\Theta(x, t; q)], \tag{12}$$

where the Laplace transform is designated by \mathcal{L} , the initial guess of $u(x, t)$ is represented as $u_0(x, t)$, and the auxiliary parameter $\hbar \neq 0$. In the following, we present the conclusions for $q = \frac{1}{n}$ and $q = 0$, respectively,

$$\Theta(x, t; \frac{1}{n}) = u(x, t), \quad \Theta(x, t; 0) = u_0(x, t). \tag{13}$$

The solutions $\Theta(x, t; q)$ converge to solutions $u(x, t)$ from the initial guess $u_0(x, t)$ as the embedding parameter q increases from 0 to $\frac{1}{n}$. Employing Taylor’s theorem [28] about q , the series expansion of function $\Theta(x, t; q)$ is given,

$$\Theta(x, t; q) = u_0(x, t) + \sum_{l=1}^{\infty} u_l(x, t)q^l, \tag{14}$$

where

$$u_l(x, t) = \frac{1}{l!} \frac{\partial^l \Theta(x, t; q)}{\partial q^l} \Big|_{q=0}. \tag{15}$$

If Equation (14) converges at $q = \frac{1}{n}$ and the initial guess u_0 , asymptotic parameter n , and auxiliary parameter \hbar values are set appropriately,

$$u(x, t) = \lim_{q \rightarrow \frac{1}{n}} \Theta(x, t; q) = \sum_{l=0}^{\infty} u_l(x, t) \left(\frac{1}{n}\right)^l. \tag{16}$$

Dividing Equation (12) by $l!$ after differentiating it l times concerning q . Finalize by taking $q = 0$ and becoming,

$$\mathcal{L}[u_l(x, t) - k_l u_{l-1}(x, t)] = \hbar H(x, t)\mathcal{R}_l(\vec{u}_{l-1}), \tag{17}$$

here

$$\vec{u}_l = \{u_0, u_1 \cdots, u_l\}. \tag{18}$$

The inverse Laplace transform acts on Equation (17), which becomes

$$u_l(x, t) = k_l u_{l-1}(x, t) + \hbar H(x, t)\mathcal{L}^{-1}[\mathcal{R}_l(\vec{u}_{l-1})], \tag{19}$$

where

$$\mathcal{R}_l(\vec{u}_{l-1}) = \frac{1}{(l-1)!} \frac{\partial^{l-1} \mathcal{B}(\Theta(x, t; q))}{\partial q^{l-1}} \Big|_{q=0}, \quad k_l = \begin{cases} 0, & l \leq 1, \\ n, & l > 1. \end{cases} \tag{20}$$

To acquire the iteration terms of $u_l(x, t)$, our suggested technique employs homotopy polynomials to provide a unique correction function. The numerical solutions for q-HATM series are

$$u^{[M]}(x, t) = \sum_{l=0}^M u_l(x, t) \left(\frac{1}{n}\right)^l. \tag{21}$$

2.3. Convergence Analysis of the q-HATM

The recommended approach has been employed during this study to investigate the convergence of Equation (8).

Theorem 1 (Uniqueness theorem). *For any α in $(0, 1)$, where $\gamma = \hbar(\lambda + \mu)T + n + \hbar$, the solution of Equation (8) generated employing the q-HATM is unique.*

Proof. The solution to Equation (8) is expressed as

$$u(x, t) = \sum_{l=0}^{\infty} u_l(x, t) \left(\frac{1}{n}\right)^l, \tag{22}$$

where

$$u_l(x, t) = \hbar \mathcal{L}^{-1} \left[\frac{1}{s} \mathcal{L} [Nu(x, t) + Ru(x, u)] + (k_l + \hbar)u_{l-1}(x, t) - \left(1 - \frac{k_l}{n}\right) \frac{1}{s} [u(x, 0) + f(x, t)] \right]. \tag{23}$$

Assuming that the two solutions to Equation (8) are u and u^Δ , the above equation yields the following result:

$$|u - u^\Delta| = |\hbar \mathcal{L}^{-1} \left[\frac{1}{s} \mathcal{L} [N(u - u^\Delta) + R(u - u^\Delta)] + (n + \hbar)(u - u^\Delta) \right]|. \tag{24}$$

It follows from the Laplace convolution theorem [29] that we possess

$$\begin{aligned} |u - u^\Delta| &\leq \hbar \int_0^t (|N(u - u^\Delta)| + |R(u - u^\Delta)|)(t - \tau) d\tau + (n + \hbar)|u - u^\Delta| \\ &\leq \hbar \int_0^t (\lambda + \mu)|u - u^\Delta|(t - \tau) d\tau + (n + \hbar)|u - u^\Delta|. \end{aligned} \tag{25}$$

Further, making use of the integral mean value theorem [30],

$$\begin{aligned} |u - u^\Delta| &\leq \hbar(\lambda + \mu)|u - u^\Delta|T + (n + \hbar)|u - u^\Delta| \\ &\leq \gamma|u - u^\Delta|, \end{aligned} \tag{26}$$

where $\gamma = \hbar(\lambda + \mu)T + n + \hbar$. This means that,

$$|u - u^\Delta| \leq \gamma|u - u^\Delta| \quad \Rightarrow \quad (\gamma - 1)|u - u^\Delta| \geq 0, \tag{27}$$

as $0 < \gamma < 1$; then, $u = u^\Delta$. As a result, Equation (8) has a unique solution. \square

Theorem 2 (Convergence theorem). *Considering that $Q : X \rightarrow X$ is a nonlinear mapping, alongside X , in this case, being a Banach space, this allows for*

$$\|Q(u) - Q(w)\| \leq \gamma\|u - w\|, \quad \forall u, w \in X. \tag{28}$$

In line with Banach’s theory [31] of fixed points, Q has a fixed point. The sequence generated via the q -HATM similarly converges to the fixed point of Q for u_0 and w_0 , which has been selected at random among X , and

$$\|u_l - u_n\| \leq \frac{\gamma^n}{1 - \gamma} \|u_1 - u_0\|, \quad \forall u_0, w_0 \in X. \tag{29}$$

Proof. The norm is denoted by $\|g(t)\| = \max_{t \in J} |g(t)|$. The Banach space $(C[J], \|\cdot\|)$ includes continuous functions performed on J . As previously mentioned, the sequence $\{u_n\}$ is a Cauchy-like sequence in the Banach space X ,

$$\begin{aligned} \|u_l - u_n\| &= \max_{t \in J} |u_l - u_n| \\ &= \max_{t \in J} |\hbar \mathcal{L}^{-1}[\frac{1}{s} \mathcal{L}[N(u_{l-1} - u_{n-1}) + R(u_{l-1} - u_{n-1})]] + (n + \hbar)(u_{l-1} - u_{n-1})| \\ &\leq \max_{t \in J} [\hbar \mathcal{L}^{-1}[\frac{1}{s} \mathcal{L}[|N(u_{l-1} - u_{n-1})| + |R(u_{l-1} - u_{n-1})|]] + (n + \hbar)|u_{l-1} - u_{n-1}|]. \end{aligned} \tag{30}$$

The Laplace transform’s convolution theorem allows the following:

$$\begin{aligned} \|u_l - u_n\| &\leq \max_{t \in J} [\hbar \int_0^t [|N(u_{l-1} - u_{n-1})| + |R(u_{l-1} - u_{n-1})|](t - \tau) d\tau + (n + \hbar)|u_{l-1} - u_{n-1}|] \\ &\leq \max_{t \in J} [\hbar \int_0^t [(\lambda + \mu)|u_{l-1} - u_{n-1}|](t - \tau) d\tau + (n + \hbar)|u_{l-1} - u_{n-1}|]. \end{aligned} \tag{31}$$

Following that, implementing the integral mean value theorem,

$$\begin{aligned} \|u_l - u_n\| &\leq \max_{t \in J} [\hbar(\lambda + \mu)|u_{l-1} - u_{n-1}|T + (n + \hbar)|u_{l-1} - u_{n-1}|] \\ &\leq \gamma \|u_{l-1} - u_{n-1}\| \Leftrightarrow \gamma = \hbar(\lambda + \mu)T + n + \hbar. \end{aligned} \tag{32}$$

If $l = n + 1$, then the situation is as follows:

$$\|u_{n+1} - u_n\| \leq \gamma \|u_n - u_{n-1}\| \leq \gamma^2 \|u_{n-1} - u_{n-2}\| \leq \dots \leq \gamma^n \|u_1 - u_0\|. \tag{33}$$

Employing the trigonometric inequality produces

$$\begin{aligned} \|u_l - u_n\| &= \|u_{n+1} - u_n + u_{n+2} - u_{n+1} + \dots + u_l - u_{l-1}\| \\ &\leq \|u_{n+1} - u_n\| + \|u_{n+2} - u_{n+1}\| + \dots + \|u_l - u_{l-1}\| \\ &\leq [\gamma^n + \gamma^{n+1} + \dots + \gamma^{l-1}] \|u_1 - u_0\| \\ &\leq \gamma^n \times [1 + \gamma + \dots + \gamma^{l-n-1}] \|u_1 - u_0\| \\ &\leq \gamma^n \times \frac{1 - \gamma^{l-n-1}}{1 - \gamma} \|u_1 - u_0\|. \end{aligned} \tag{34}$$

Since $0 < \gamma < 1$, then $1 - \gamma^{l-n-1} < 1$, and we have

$$\|u_l - u_n\| \leq \frac{\gamma^n}{1 - \gamma} \|u_1 - u_0\|. \tag{35}$$

However, $\|u_1 - u_0\| < \infty$, so as $l \rightarrow \infty$, then $\|u_l - u_n\| \rightarrow 0$. Given that all Cauchy sequences are convergent, the sequence $\{u_n\}$ in the Banach space $C[J]$ is a Cauchy sequence. \square

Theorem 3. The utmost absolute truncation error will be calculated as follows if there is a real number $0 < \gamma < 1$ and $\|u_{l+1}\| \leq \gamma \|u_l\|$ is satisfied:

$$\|u(x, t) - u^{[M]}(x, t)\| \leq \frac{\gamma^{M+1}}{n^M(n - \gamma)} \|u_0(x, t)\|. \tag{36}$$

Proof. Given the values of n ($n \geq 1$) and \hbar ($\hbar \neq 0$), we have

$$\begin{aligned}
 \|u(x, t) - u^{[M]}(x, t)\| &= \left\| \sum_{l=0}^{\infty} u_l(x, t) \left(\frac{1}{n}\right)^l - \sum_{l=0}^M u_l(x, t) \left(\frac{1}{n}\right)^l \right\| \\
 &\leq \sum_{l=M+1}^{\infty} \|u_l(x, t)\| \left(\frac{1}{n}\right)^l \\
 &\leq \sum_{l=M+1}^{\infty} \gamma^l \|u_0(x, t)\| \left(\frac{1}{n}\right)^l \\
 &\leq \sum_{l=M+1}^{\infty} \left(\frac{\gamma}{n}\right)^l \|u_0(x, t)\| \\
 &\leq \left(\frac{\gamma}{n}\right)^{M+1} \left[1 + \frac{\gamma}{n} + \left(\frac{\gamma}{n}\right)^2 + \dots\right] \|u_0(x, t)\| \\
 &\leq \left(\frac{\gamma}{n}\right)^{M+1} \frac{1}{1 - \frac{\gamma}{n}} \|u_0(x, t)\| \\
 &= \frac{\gamma^{M+1}}{n^M(n - \gamma)} \|u_0(x, t)\|.
 \end{aligned}
 \tag{37}$$

This proof of the theorem has now been finished. \square

3. Applications of the Extended Three-Coupled Korteweg–de Vries System

3.1. Analytical Solutions for Equation (1)

We right now utilize the sub equation approach to discover the analytical solutions to Equation (1). As a consequence, we perform the wave transformation described below,

$$\eta = bt + x, \quad u(x, t) = U(\eta), \quad v(x, t) = V(\eta), \quad w(x, t) = W(\eta).
 \tag{38}$$

Here are the simplified ODEs that result from inserting Equation (38) into Equation (1),

$$\begin{aligned}
 bU' &= \beta_1 U''' + \beta_2 U'V + \beta_2 UV', \\
 bV' &= \beta_1 \beta_3 V''' + 2\beta_2 \beta_3 VV' - \beta_2 W', \\
 bW' &= \beta_1 W''' + \beta_2 VW' - 2\beta_2 UU'.
 \end{aligned}
 \tag{39}$$

The homogeneous balance between the nonlinear item and the highest-order derivative has to be obtained by Equation (39), which results in the following solutions,

$$\begin{aligned}
 U(\eta) &= a_0 + a_1 \psi(\eta) + a_2 \psi^2(\eta), \\
 V(\eta) &= b_0 + b_1 \psi(\eta) + b_2 \psi^2(\eta), \\
 W(\eta) &= c_0 + c_1 \psi(\eta) + c_2 \psi^2(\eta).
 \end{aligned}
 \tag{40}$$

The following solutions are derived by computing the system of equations created by substituting Equation (40) into Equation (39),

$$\begin{aligned}
 a_0 &= -\frac{a_2(-144\alpha\beta_1^3 - 18b_0\beta_1^2\beta_2 + a_2^2\beta_2^3 + 144\alpha\beta_1^3\beta_3 + 36b_0\beta_1^2\beta_2\beta_3)}{108\beta_1^3}, & a_1 &= 0, \\
 b_2 &= -\frac{6\beta_1}{\beta_2}, \quad c_2 = \frac{a_2^2\beta_2}{3\beta_1}, \quad b_1 = 0, \quad c_1 = 0, \quad b = \frac{a_2^2\beta_2^3 + 144\alpha\beta_1^3\beta_3 + 36b_0\beta_1^2\beta_2\beta_3}{18\beta_1^2},
 \end{aligned}
 \tag{41}$$

where $a_2, b_0,$ and c_0 are arbitrary constants. In other words, we acquire three different travelling wave solutions for Equation (1): a soliton solution with $\alpha < 0,$

$$\begin{aligned}
 u(x, t) &= -\frac{a_2(-144\alpha\beta_1^3 - 18b_0\beta_1^2\beta_2 + a_2^2\beta_2^3 + 144\alpha\beta_1^3\beta_3 + 36b_0\beta_1^2\beta_2\beta_3)}{108\beta_1^3} \\
 &\quad - a_2\alpha \tanh^2\left(\sqrt{-\alpha}\left(x + \frac{a_2^2\beta_2^3 + 144\alpha\beta_1^3\beta_3 + 36b_0\beta_1^2\beta_2\beta_3}{18\beta_1^2}t\right)\right), \\
 v(x, t) &= b_0 + \frac{6\beta_1}{\beta_2}\alpha \tanh^2\left(\sqrt{-\alpha}\left(x + \frac{a_2^2\beta_2^3 + 144\alpha\beta_1^3\beta_3 + 36b_0\beta_1^2\beta_2\beta_3}{18\beta_1^2}t\right)\right), \\
 w(x, t) &= c_0 - \frac{a_2^2\beta_2}{3\beta_1}\alpha \tanh^2\left(\sqrt{-\alpha}\left(x + \frac{a_2^2\beta_2^3 + 144\alpha\beta_1^3\beta_3 + 36b_0\beta_1^2\beta_2\beta_3}{18\beta_1^2}t\right)\right),
 \end{aligned}
 \tag{42}$$

a periodic solution with $\alpha > 0,$

$$\begin{aligned}
 u(x, t) &= -\frac{a_2(-144\alpha\beta_1^3 - 18b_0\beta_1^2\beta_2 + a_2^2\beta_2^3 + 144\alpha\beta_1^3\beta_3 + 36b_0\beta_1^2\beta_2\beta_3)}{108\beta_1^3} \\
 &\quad + a_2\alpha \tan^2\left(\sqrt{\alpha}\left(x + \frac{a_2^2\beta_2^3 + 144\alpha\beta_1^3\beta_3 + 36b_0\beta_1^2\beta_2\beta_3}{18\beta_1^2}t\right)\right), \\
 v(x, t) &= b_0 - \frac{6\beta_1}{\beta_2}\alpha \tan^2\left(\sqrt{\alpha}\left(x + \frac{a_2^2\beta_2^3 + 144\alpha\beta_1^3\beta_3 + 36b_0\beta_1^2\beta_2\beta_3}{18\beta_1^2}t\right)\right), \\
 w(x, t) &= c_0 + \frac{a_2^2\beta_2}{3\beta_1}\alpha \tan^2\left(\sqrt{\alpha}\left(x + \frac{a_2^2\beta_2^3 + 144\alpha\beta_1^3\beta_3 + 36b_0\beta_1^2\beta_2\beta_3}{18\beta_1^2}t\right)\right),
 \end{aligned}
 \tag{43}$$

and a rational solution with $\alpha = 0,$

$$\begin{aligned}
 u(x, t) &= -\frac{a_2(-18b_0\beta_1^2\beta_2 + a_2^2\beta_2^3 + 36b_0\beta_1^2\beta_2\beta_3)}{108\beta_1^3} + a_2\left(\frac{18\beta_1^2}{18\beta_1^2x + a_2^2\beta_2^3 + 36b_0\beta_1^2\beta_2\beta_3}\right)^2, \\
 v(x, t) &= b_0 - \frac{6\beta_1}{\beta_2}\left(\frac{18\beta_1^2}{18\beta_1^2x + a_2^2\beta_2^3 + 36b_0\beta_1^2\beta_2\beta_3}\right)^2, \\
 w(x, t) &= c_0 + \frac{a_2^2\beta_2}{3\beta_1}\left(\frac{18\beta_1^2}{18\beta_1^2x + a_2^2\beta_2^3 + 36b_0\beta_1^2\beta_2\beta_3}\right)^2.
 \end{aligned}
 \tag{44}$$

3.2. Numerical Solutions for Equation (1)

Take Equation (1), for example,

$$\begin{aligned}
 u_t &= \beta_1u_{xxx} + \beta_2u_xv + \beta_2uv_x, \\
 v_t &= \beta_1\beta_3v_{xxx} + 2\beta_2\beta_3vv_x - \beta_2w_x, \\
 w_t &= \beta_1w_{xxx} + \beta_2vw_x - 2\beta_2uu_x,
 \end{aligned}
 \tag{45}$$

with initial conditions

$$\begin{aligned}
 u(x, 0) &= -\frac{a_2(-144\alpha\beta_1^3 - 18b_0\beta_1^2\beta_2 + a_2^2\beta_2^3 + 144\alpha\beta_1^3\beta_3 + 36b_0\beta_1^2\beta_2\beta_3)}{108\beta_1^3} - a_2\alpha \tanh^2(\sqrt{-\alpha}x), \\
 v(x, 0) &= b_0 + \frac{6\beta_1}{\beta_2}\alpha \tanh^2(\sqrt{-\alpha}x), \quad w(x, 0) = c_0 - \frac{a_2^2\beta_2}{3\beta_1}\alpha \tanh^2(\sqrt{-\alpha}x).
 \end{aligned}
 \tag{46}$$

When the starting conditions from Equation (46) are coupled with the Laplace transform from Equation (45), we obtain

$$\begin{aligned} \mathcal{L}[u(x, t)] &= \frac{1}{s} \mathcal{L}[\beta_1 \frac{\partial^3 u}{\partial x^3} + \beta_2 \frac{\partial u}{\partial x} v + \beta_2 u \frac{\partial v}{\partial x}] + \frac{1}{s} u(x, 0), \\ \mathcal{L}[v(x, t)] &= \frac{1}{s} \mathcal{L}[\beta_1 \beta_3 \frac{\partial^3 v}{\partial x^3} + 2\beta_2 \beta_3 v \frac{\partial v}{\partial x} - \beta_2 \frac{\partial w}{\partial x}] + \frac{1}{s} v(x, 0), \\ \mathcal{L}[w(x, t)] &= \frac{1}{s} \mathcal{L}[\beta_1 \frac{\partial^3 w}{\partial x^3} + \beta_2 v \frac{\partial w}{\partial x} - 2\beta_2 u \frac{\partial u}{\partial x}] + \frac{1}{s} w(x, 0). \end{aligned} \tag{47}$$

The following formula is used to create the zero-order deformation equation, where $i = 1, 2, 3$, and $\Theta_i(x, t; q) = \Theta_i$, respectively,

$$\begin{aligned} (1 - nq) \mathcal{L}[\Theta_1 - u_0(x, t)] &= \hbar q H(x, t) \mathcal{B}_1(\Theta_1, \Theta_2, \Theta_3), \\ (1 - nq) \mathcal{L}[\Theta_2 - v_0(x, t)] &= \hbar q H(x, t) \mathcal{B}_2(\Theta_1, \Theta_2, \Theta_3), \\ (1 - nq) \mathcal{L}[\Theta_3 - w_0(x, t)] &= \hbar q H(x, t) \mathcal{B}_3(\Theta_1, \Theta_2, \Theta_3). \end{aligned} \tag{48}$$

The nonlinear operators are:

$$\begin{aligned} \mathcal{B}_1(\Theta_1, \Theta_2, \Theta_3) &= \mathcal{L}[\Theta_1] - \frac{1}{s} u(x, 0) - \frac{1}{s} \mathcal{L}[\beta_1 \frac{\partial^3 \Theta_1}{\partial x^3} + \beta_2 \frac{\partial \Theta_1}{\partial x} \Theta_2 + \beta_2 \Theta_1 \frac{\partial \Theta_2}{\partial x}], \\ \mathcal{B}_2(\Theta_1, \Theta_2, \Theta_3) &= \mathcal{L}[\Theta_2] - \frac{1}{s} v(x, 0) - \frac{1}{s} \mathcal{L}[\beta_1 \beta_3 \frac{\partial^3 \Theta_2}{\partial x^3} + 2\beta_2 \beta_3 \Theta_2 \frac{\partial \Theta_2}{\partial x} - \beta_2 \frac{\partial \Theta_3}{\partial x}], \\ \mathcal{B}_3(\Theta_1, \Theta_2, \Theta_3) &= \mathcal{L}[\Theta_3] - \frac{1}{s} w(x, 0) - \frac{1}{s} \mathcal{L}[\beta_1 \frac{\partial^3 \Theta_3}{\partial x^3} + \beta_2 \Theta_2 \frac{\partial \Theta_3}{\partial x} - 2\beta_2 \Theta_1 \frac{\partial \Theta_1}{\partial x}]. \end{aligned} \tag{49}$$

The algorithm which has been proposed as follows has been employed to calculate the m -order deformation equation,

$$\begin{aligned} \mathcal{L}[u_l(x, t) - k_l u_{l-1}(x, t)] &= \hbar \mathcal{R}_{1, l}(\vec{u}_{l-1}, \vec{v}_{l-1}, \vec{w}_{l-1}), \\ \mathcal{L}[v_l(x, t) - k_l v_{l-1}(x, t)] &= \hbar \mathcal{R}_{2, l}(\vec{u}_{l-1}, \vec{v}_{l-1}, \vec{w}_{l-1}), \\ \mathcal{L}[w_l(x, t) - k_l w_{l-1}(x, t)] &= \hbar \mathcal{R}_{3, l}(\vec{u}_{l-1}, \vec{v}_{l-1}, \vec{w}_{l-1}), \end{aligned} \tag{50}$$

where

$$\begin{aligned} \mathcal{R}_{1, l}(\vec{u}_{l-1}, \vec{v}_{l-1}, \vec{w}_{l-1}) &= \mathcal{L}[u_{l-1}(x, t)] - (1 - \frac{k_l}{n}) \frac{1}{s} u(x, 0) \\ &\quad - \frac{1}{s} \mathcal{L}[\beta_1 \frac{\partial^3 u_{l-1}}{\partial x^3} + \beta_2 \sum_{k=0}^{l-1} v_k \frac{\partial u_{l-1-k}}{\partial x} + \beta_2 \sum_{k=0}^{l-1} u_k \frac{\partial v_{l-1-k}}{\partial x}], \\ \mathcal{R}_{2, l}(\vec{u}_{l-1}, \vec{v}_{l-1}, \vec{w}_{l-1}) &= \mathcal{L}[v_{l-1}(x, t)] - (1 - \frac{k_l}{n}) \frac{1}{s} v(x, 0) \\ &\quad - \frac{1}{s} \mathcal{L}[\beta_1 \beta_3 \frac{\partial^3 v_{l-1}}{\partial x^3} + 2\beta_2 \beta_3 \sum_{k=0}^{l-1} v_k \frac{\partial v_{l-1-k}}{\partial x} - \beta_2 \frac{\partial w_{l-1}}{\partial x}], \\ \mathcal{R}_{3, l}(\vec{u}_{l-1}, \vec{v}_{l-1}, \vec{w}_{l-1}) &= \mathcal{L}[w_{l-1}(x, t)] - (1 - \frac{k_l}{n}) \frac{1}{s} w(x, 0) \\ &\quad - \frac{1}{s} \mathcal{L}[\beta_1 \frac{\partial^3 w_{l-1}}{\partial x^3} + \beta_2 \sum_{k=0}^{l-1} v_k \frac{\partial w_{l-1-k}}{\partial x} - 2\beta_2 \sum_{k=0}^{l-1} u_k \frac{\partial u_{l-1-k}}{\partial x}]. \end{aligned} \tag{51}$$

In Equation (50), we can utilize the inverse Laplace transform to deduce

$$\begin{aligned} u_l(x, t) &= k_l u_{l-1}(x, t) + \hbar \mathcal{L}^{-1} \mathcal{R}_{1, l}(\vec{u}_{l-1}, \vec{v}_{l-1}, \vec{w}_{l-1}), \\ v_l(x, t) &= k_l v_{l-1}(x, t) + \hbar \mathcal{L}^{-1} \mathcal{R}_{2, l}(\vec{u}_{l-1}, \vec{v}_{l-1}, \vec{w}_{l-1}), \\ w_l(x, t) &= k_l w_{l-1}(x, t) + \hbar \mathcal{L}^{-1} \mathcal{R}_{3, l}(\vec{u}_{l-1}, \vec{v}_{l-1}, \vec{w}_{l-1}). \end{aligned} \tag{52}$$

The following results have been achieved by dealing with the equations provided earlier,

$$\begin{aligned}
 u_0(x, t) &= -\frac{a_2(-144\alpha\beta_1^3 - 18b_0\beta_1^2\beta_2 + a_2^2\beta_2^3 + 144\alpha\beta_1^3\beta_3 + 36b_0\beta_1^2\beta_2\beta_3)}{108\beta_1^3} - a_2\alpha\tanh^2(\sqrt{-\alpha}x), \\
 v_0(x, t) &= b_0 + \frac{6\beta_1}{\beta_2}\alpha\tanh^2(\sqrt{-\alpha}x), \\
 w_0(x, t) &= c_0 - \frac{a_2^2\beta_2}{3\beta_1}\alpha\tanh^2(\sqrt{-\alpha}x), \\
 u_1(x, t) &= \frac{\sqrt{-\alpha}a_2ht \tanh(\sqrt{-\alpha}x)\operatorname{sech}^2(\sqrt{-\alpha}x)(a_2^2\beta_2^3 + 36\beta_1^2\beta_3(4\alpha\beta_1 + b_0\beta_2))}{9\beta_1^2}, \\
 v_1(x, t) &= -\frac{2\sqrt{-\alpha}ht \tanh(\sqrt{-\alpha}x)\operatorname{sech}^2(\sqrt{-\alpha}x)(a_2^2\beta_2^3 + 36\beta_1^2\beta_3(4\alpha\beta_1 + b_0\beta_2))}{3\beta_1\beta_2}, \\
 w_1(x, t) &= -\frac{\beta_2(\beta_2^3 + 36\beta_1^2(\beta_2 - 4\beta_1)\beta_3)ht \tanh(x)\operatorname{sech}^2(x)}{27\beta_1^3}, \\
 &\vdots
 \end{aligned}
 \tag{53}$$

Similar calculations can be carried out for the remaining iteration terms. Finally, the numerical solutions of Equation (45) are supplied as

$$\begin{aligned}
 u^{[M]}(x, t) &= u_0(x, t) + \sum_{l=1}^M u_l(x, t)\left(\frac{1}{n}\right)^l, \\
 v^{[M]}(x, t) &= v_0(x, t) + \sum_{l=1}^M v_l(x, t)\left(\frac{1}{n}\right)^l, \\
 w^{[M]}(x, t) &= w_0(x, t) + \sum_{l=1}^M w_l(x, t)\left(\frac{1}{n}\right)^l.
 \end{aligned}
 \tag{54}$$

As $N \rightarrow \infty$, the numerical solutions for Equation (1) correspondingly converge to the analytical solutions of Equation (45) for $n = 1$ and $\hbar = -1$.

4. Numerical Results and Simulation

With the q-HATM results in mind, the extended three-coupled Korteweg–de Vries system will be numerically simulated in this section. The comparisons between numerical solutions and analytical solutions generated by q-HATM with a five-term approximation are shown in Figures 1–3. The absolute error function of Equation (1) is shown in Figure 4. The \hbar curves are shown in Figures 5–7 for distinct n and x values. By altering the horizontal line in the \hbar curve, which symbolizes the convergence range of the extended coupled Korteweg–de Vries system, we may change the convergence range of the series solutions. Figures 5–7 emphatically demonstrate that the numerical solutions converge in the intervals $(-2.1, 0.1)$ and $(-3.8, 0.2)$ for $n = 1$ and $n = 2$, respectively. As a result, we discovered that the range of the permitted \hbar convergence interval is wider when $n = 3$. Figures 5–7 demonstrate that when the n value increases, the convergence range also does. The comparisons between numerical solutions and analytical solutions are displayed in Tables 1–3. These charts show the accuracy of the results of the proposed method.

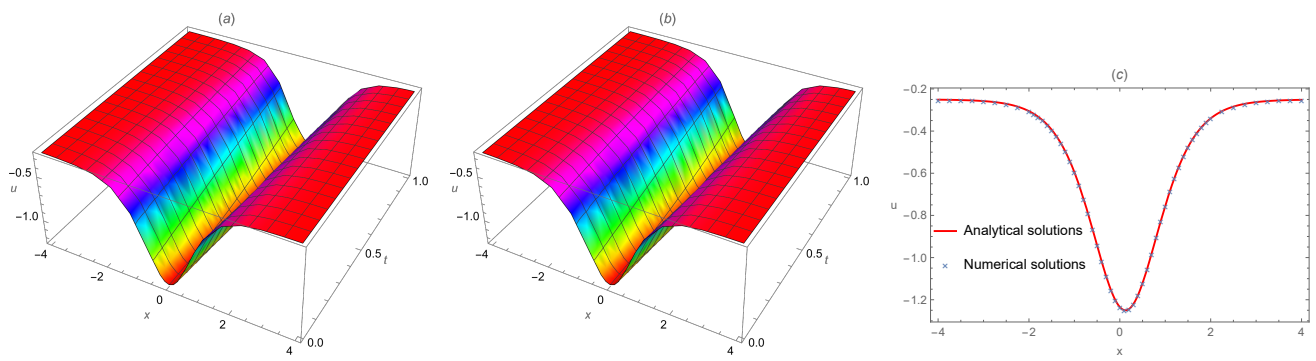


Figure 1. (a) Numerical solutions. (b) Analytical solutions. (c) Comparison of numerical solutions and analytical solutions at $n = 1$ and $\hbar = -1$ for Equation (1).

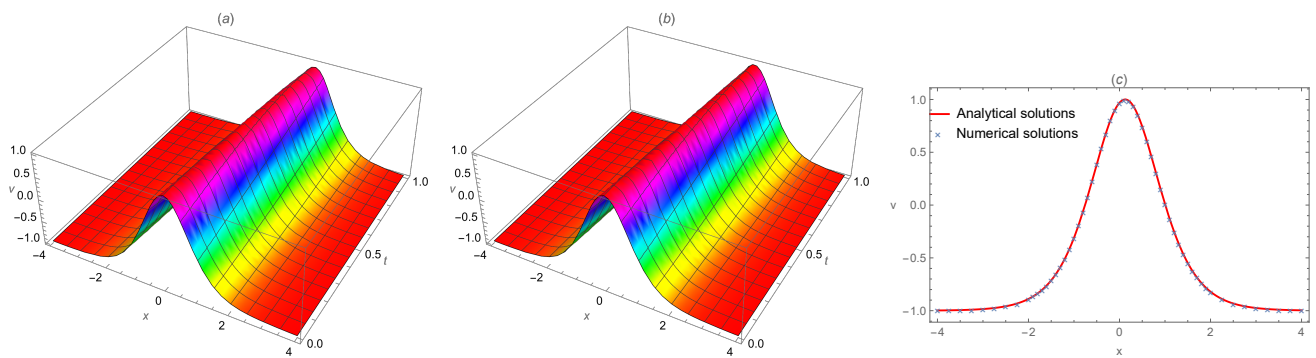


Figure 2. (a) Numerical solutions. (b) Analytical solutions. (c) Comparison of numerical solutions and analytical solutions at $n = 1$ and $\hbar = -1$ for Equation (1).

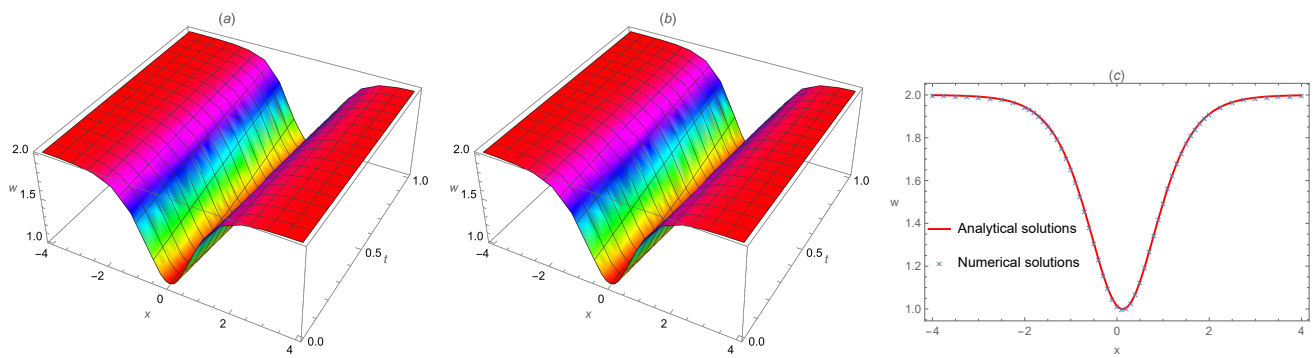


Figure 3. (a) Numerical solutions. (b) Analytical solutions. (c) Comparison of numerical solutions and analytical solutions at $n = 1$ and $\hbar = -1$ for Equation (1).

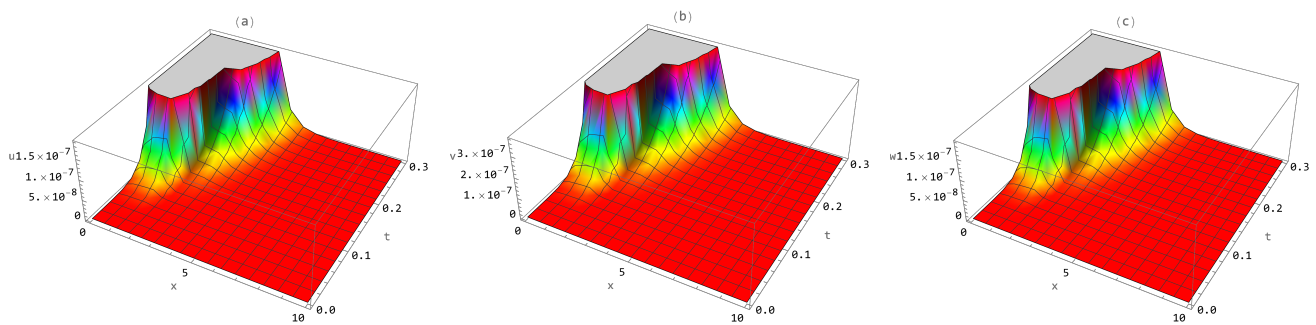


Figure 4. Surface of (a) absolute error = $|u_{exa.} - u_{num.}|$. (b) Absolute error = $|v_{exa.} - v_{num.}|$. (c) Absolute error = $|w_{exa.} - w_{num.}|$ at $n = 1$ and $\hbar = -1$ of Equation (1).

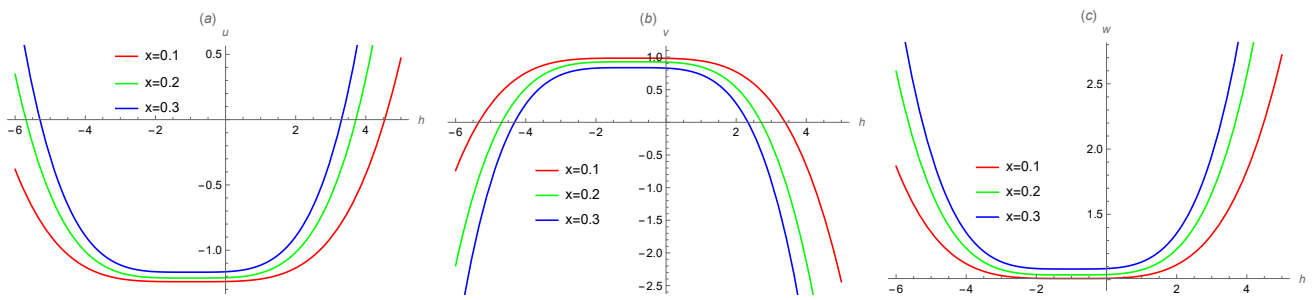


Figure 5. When $n = 1$ and $t = 0.01$, the outline of (a) numerical solutions u , (b) numerical solutions v , and (c) numerical solutions w with different x values.

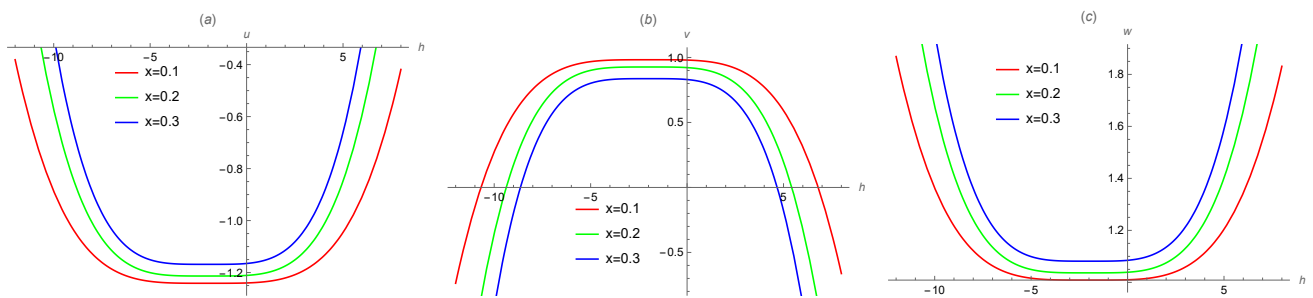


Figure 6. When $n = 2$ and $t = 0.01$, the outline of (a) numerical solutions u , (b) numerical solutions v , and (c) numerical solutions w with different x values.

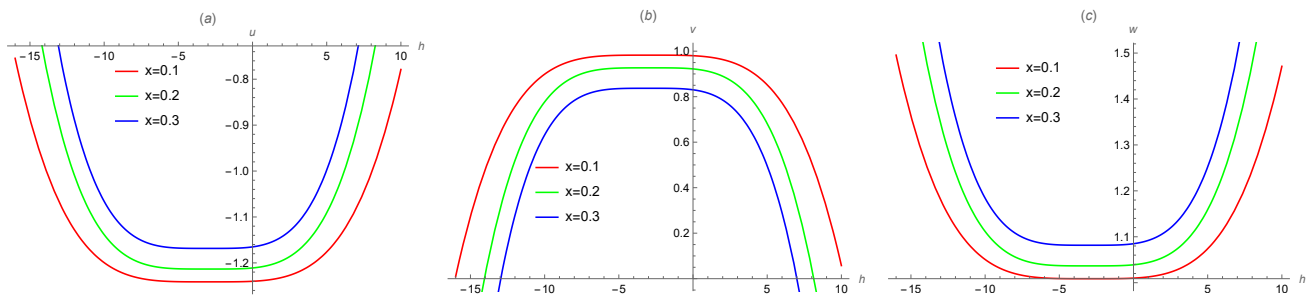


Figure 7. When $n = 3$ and $t = 0.01$, the outline of (a) numerical solutions u , (b) numerical solutions v , and (c) numerical solutions w with different x values.

Table 1. Numerical results for numerical and analytical solutions of $u(x, t)$ when $n = 1$ and $\hbar = -1$.

t	x	Numerical	Exact	Absolute Error
0.1	-10	-0.25000001	-0.25000001	1.99840×10^{-15}
	-5	-0.25016025	-0.25016025	4.51094×10^{-11}
	0	-1.24610392	-1.24610390	2.24716×10^{-8}
	5	-0.25020576	-0.25020576	4.70228×10^{-11}
	10	-0.25000001	-0.25000000	2.10942×10^{-15}
0.2	-10	-0.25000001	-0.25000001	6.45040×10^{-14}
	-5	-0.25014142	-0.25014142	1.41446×10^{-9}
	0	-1.23453776	-1.23453633	1.42947×10^{-6}
	5	-0.25023315	-0.25023315	1.53703×10^{-9}
	10	-0.25000001	-0.25000001	6.99441×10^{-14}

Table 2. Numerical results for numerical and analytical solutions of $v(x, t)$ when $n = 1$ and $\hbar = -1$.

t	x	Numerical	Exact	Absolute Error
0.1	-10	-0.99999999	-0.99999999	4.02223×10^{-15}
	-5	-0.99967950	-0.99967950	9.02187×10^{-11}
	0	0.99220785	0.99220780	4.49431×10^{-8}
	5	-0.99958848	-0.99958848	9.40457×10^{-11}
	10	-0.99999998	-0.99999998	4.20917×10^{-15}
0.2	-10	-0.99999999	-0.99999999	1.28923×10^{-13}
	-5	-0.99971716	-0.99971716	2.82892×10^{-9}
	0	0.96907552	0.96907266	2.85893×10^{-6}
	5	-0.99953370	-0.99953370	3.07407×10^{-9}
	10	-0.99999998	-0.99999998	1.39870×10^{-13}

Table 3. Numerical results for numerical and analytical solutions of $w(x, t)$ when $n = 1$ and $\hbar = -1$.

t	x	Numerical	Exact	Absolute Error
0.1	-10	1.99999999	1.99999999	2.01112×10^{-15}
	-5	1.99983975	1.99983975	4.51093×10^{-11}
	0	1.00389608	1.00389610	2.24716×10^{-8}
	5	1.99979424	1.99979424	4.70228×10^{-11}
	10	1.99999999	1.99999999	2.10459×10^{-15}
0.2	-10	1.99999999	1.99999999	6.44650×10^{-14}
	-5	1.99985858	1.99985858	1.41446×10^{-9}
	0	1.01546224	1.01546367	1.42947×10^{-6}
	5	1.99976685	1.99976685	1.53703×10^{-9}
	10	1.99999999	1.99999999	6.99350×10^{-14}

5. Conclusions

In the current study, the q-HATM and the Laplace transform have been employed to evaluate numerical solutions of an extended coupled Korteweg–de Vries system. The suggested technique has the benefit of not necessitating any discretization, linearization, or interference. The asymptotic parameter n and auxiliary parameter \hbar have been incorporated in the numerical solutions of the q-HATM, which provides us with a rapid means to modify the convergence speed and range within the found series solutions. The numerical outcomes show what a successful, accurate, and robust procedure iteration is for solving PDEs. Finally, we can prove that the proposed method is more systematic and accurate, and it can be used to study the complicated processes of nonlinear phenomena.

Author Contributions: Conceptualization, P.W. and X.F.; software, P.W.; investigation, P.W.; data curation, X.F.; writing—original draft preparation, P.W.; writing—review and editing, P.W. and X.F.; supervision, X.F.; funding acquisition, X.F. All authors have read and agreed to the published version of the manuscript.

Funding: This research received no external funding.

Data Availability Statement: The material of this article includes the data reported in this study.

Conflicts of Interest: The authors declare no conflict of interest.

References

1. Leung, A.W. *Systems of Nonlinear Partial Differential Equations: Applications to Biology and Engineering*; Springer Science Business Media: Dordrecht, The Netherlands, 2013.
2. Inc, M.; Yusuf, A.; Aliyu, A.I.; Baleanu, D. Soliton solutions and stability analysis for some conformable nonlinear partial differential equations in mathematical physics. *Opt. Quantum Electron.* **2018**, *50*, 190. [[CrossRef](#)]
3. Zayed, E.M.E.; Arnous, A.H. Exact Traveling Wave Solutions of Nonlinear PDEs in Mathematical Physics Using the Modified Simple Equation Method. *Appl. Appl. Math.* **2013**, *8*, 553–572.

4. Boureghda, A. Numerical solution of the oxygen diffusion in absorbing tissue with a moving boundary. *Commun. Numer. Methods Eng.* **2006**, *22*, 933–942. [[CrossRef](#)]
5. Botmart, T.; Alotaibi, B.M.; Shah, R.; El-Sherif, L.S.; El-Tantawy, S.A. A Reliable Way to Deal with the Coupled Fractional Korteweg-De Vries Equations within the Caputo Operator. *Symmetry* **2022**, *14*, 2452. [[CrossRef](#)]
6. Aljahdaly, N.H.; Akgül, A.; Shah, R.; Mahariq, I.; Kafle, J. A comparative analysis of the fractional-order coupled Korteweg-De Vries equations with the Mittag-Leffler law. *J. Math.* **2022**, 8876149–8876178. [[CrossRef](#)]
7. Shah, N.A.; Alyousef, H.A.; El-Tantawy, S.A.; Shah, R.; Chung, J.D. Analytical investigation of fractional-order Korteweg-De Vries-type equations under Atangana-Baleanu-Caputo operator: Modeling nonlinear waves in a plasma and fluid. *Symmetry* **2022**, *14*, 739. [[CrossRef](#)]
8. Ma, W.-X. AKNS type reduced integrable bi-Hamiltonian hierarchies with four potentials. *Appl. Math. Lett.* **2023**, *145*, 108775. [[CrossRef](#)]
9. Ma, W.-X. Four-component integrable hierarchies of Hamiltonian equations with $(m + n + 2)$ th-order Lax pairs. *Theor. Math. Phys.* **2023**, *216*, 1180–1188. [[CrossRef](#)]
10. Liao, S. On the homotopy analysis method for nonlinear problems. *Appl. Math. Comput.* **2004**, *147*, 499–513. [[CrossRef](#)]
11. Liao, S. Series solution of nonlinear eigenvalue problems by means of the homotopy analysis method. *Nonlinear Anal. Real World Appl.* **2009**, *10*, 2455–2470. [[CrossRef](#)]
12. Liao, S.; Tan, Y. A general approach to obtain series solutions of nonlinear differential equations. *Stud. Appl. Math.* **2007**, *119*, 297–354. [[CrossRef](#)]
13. Liao, S.J. An approximate solution technique which does not depend upon small parameters: A special example. *Int. J. Non-Linear Mech.* **1995**, *30*, 371–380. [[CrossRef](#)]
14. El-Tawil, M.A.; Huseen, S.N. The Q-homotopy analysis method (QHAM). *Int. J. Appl. Math. Mech.* **2012**, *8*, 51–75.
15. Zhao, Y.; Lin, Z.; Liu, Z. The improved homotopy analysis method for the Thomas-Fermi equation. *Appl. Math Comput.* **2012**, *218*, 8363–8369. [[CrossRef](#)]
16. Mesloub, S.; Alsaud, H. Exploring the Efficiency of the q-Homotopy Analysis Transform Method for Solving a Fractional Initial Boundary Value Problem with a Nonlocal Condition. *Axioms* **2023**, *12*, 790. [[CrossRef](#)]
17. Shah, R.; Khan, H.; Baleanu, D. Fractional Whitham-Broer-Kaup equations within modified analytical approaches. *Axioms* **2019**, *8*, 125. [[CrossRef](#)]
18. Malagi, N.S.; Veerasha, P.; Prasannakumara, B.C.; Prasanna, G.D.; Prakasha, D.G. A new computational technique for the analytic treatment of time-fractional Emden Fowler equations. *Math. Comput. Simul.* **2021**, *190*, 362–376. [[CrossRef](#)]
19. Veerasha, P.; Prakasha, D.G. A novel technique for (2+1)-dimensional time-fractional coupled Burgers equations. *Math. Comput. Simul.* **2019**, *166*, 324–345. [[CrossRef](#)]
20. El-Tawil, M.A.; Huseen, S.N. On Convergence of q-Homotopy Analysis Method. *Int. J. Contemp. Math. Sci.* **2013**, *8*, 481–497. [[CrossRef](#)]
21. Veerasha, P.; Prakasha, D.G.; Kumar, D. An efficient technique for nonlinear time-fractional Klein-Fock-Gordon equation. *Appl. Math. Comput.* **2020**, *364*, 124637. [[CrossRef](#)]
22. Gao, X.Y.; Guo, Y.J.; Shan, W.-R.; Zhou, T.Y. Singular manifold, auto-Bäcklund transformations and symbolic-computation steps with solitons for an extended three-coupled Korteweg-de Vries system. *Int. J. Geom. Methods Mod. Phys.* **2022**, *19*, 2250229. [[CrossRef](#)]
23. Gao, X.Y.; Guo, Y.J.; Shan, W.R.; Zhou, T.Y. Report on an extended three-coupled Korteweg-de Vries system. *Ric. Mat.* **2023**. [[CrossRef](#)]
24. Gao, X.Y.; Guo, Y.J.; Shan, W.R. Hetero-Bäcklund transformation, bilinear forms and N solitons for a generalized three-coupled Korteweg-de Vries system. *Qual. Theory Dyn. Syst.* **2021**, *20*, 87–98. [[CrossRef](#)]
25. Ray, S.; Sahoo, S. New Exact Solutions of Fractional Zakharov-Kuznetsov and Modified Zakharov-Kuznetsov Equations Using Fractional Sub-Equation Method. *Commun. Theor. Phys.* **2015**, *63*, 25–30. [[CrossRef](#)]
26. Senol, M. Analytical and approximate solutions of (2+1)-dimensional time-fractional Burgers-Kadomtsev-Petviashvili equation. *Commun. Theor. Phys.* **2020**, *72*, 055003. [[CrossRef](#)]
27. Adel, M. Numerical simulations for the variable order two-dimensional reaction sub-diffusion equation: Linear and Nonlinear. *Fractals* **2022**, *30*, 2240019. [[CrossRef](#)]
28. Odibat, Z.M.; Shawagfeh, N.T. Generalized Taylor's formula. *Appl. Math. Comput.* **2007**, *186*, 286–293. [[CrossRef](#)]
29. Podlubny, I. *Fractional Differential Equations*; Academic Press, New York, NY, USA, **1999**.
30. Nikonorov, Y.G. On the integral mean value theorem. *Sib. Math. J.* **1993**, *34*, 150–152. [[CrossRef](#)]
31. Magrenan, A.A. A new tool to study real dynamics: The convergence plane. *Appl. Math. Comput.* **2014**, *248*, 215–224. [[CrossRef](#)]

Disclaimer/Publisher's Note: The statements, opinions and data contained in all publications are solely those of the individual author(s) and contributor(s) and not of MDPI and/or the editor(s). MDPI and/or the editor(s) disclaim responsibility for any injury to people or property resulting from any ideas, methods, instructions or products referred to in the content.